CONTRIBUTION TO IMPROVING THE PERFORMANCES OF ELECTRO-MECHANICAL ACTUATORS BASED ON SQUIRREL CAGE INDUCTION MOTOR

Z. MADDI D. AOUZELLAG
Laboratoire de Maitrise des Energies Renouvelables (LMER), Université de Bejaia, Faculté de Technologie, Email zakari.maddi@univ-bejaia.dz

Abstract: *This paper presents a contribution to improving startup performances of actuators based on deep bar induction motors (IM). To do this, modifications have been made at the rotor bars, through insertion of massive ferromagnetic pieces inside them. Two approaches have been performed (semi-analytical and numerical) to model these new proposed bars over a frequency range. A dynamic modelling has been carried out, which takes into account the influence of these pieces on different starting characteristics namely the electromagnetic torque, the stator current, the speed, and the machine startup time studied.*

Key words: *IM, deep bar, massive ferromagnetic pieces, dynamic modelling.*

1. Introduction

The IM actuators occupy the first place in the field of industrial applications and the development of mechanical power, they have become an almost exclusive alternative. For more than a century to date, research work has continued to increase, attempting to achieve a precise calculation of its parameters and to improve its performances [1, 2]. Among the most reported works in this axis, we distinguish the determination and taking into account the non-linear phenomena, which are manifested in the different operating conditions of the IM, changing thus the behavior of its parameters.

However, the most flexible phenomena are the magnetic saturation effect, which affects the magnetization reactance [3-5]. The evolution of temperature, which affects the IM parameters, by changing the behavior of the materials and inducing energy losses [6-8]. Also the skin effect, which exponentially changes the rotor impedance. This latter has incited several authors to take a particular interest by exploiting it with the aim of improving the starting and / or braking performance of electromechanical actuators. This is explained by a large number of contributions attempting a direct approach to its modelling in rotor parameters calculation [9-15]. Techniques and algorithm approaches have also been developed solely for the purpose of optimizing its consideration [16-19], others have exploited it in an indirect way by making changes in the rotor (bars shape, size and materials), in order to improve the IM starting preferences [20-24]. These research works previously quoted have largely collaborated in the improvement of the accuracy and the estimation of the non-linear phenomena, which are present in the various regimes of the motor. However, the ideal is to make improvement to its performances while reducing its energy consumption, this can be done by reducing its dimensions and/or its inrush current while maintaining its optimal performances. For this reason, this article attempted to satisfy this requirement by proposing a new original and more powerful structure of deep-bar, which has an improvement starting characteristics better than the bars currently designed and also with that of double cage.

To justify this, three modified deep bar structures (massive ferromagnetic pieces were inserted inside them) are modelled by two approaches; a field calculation and the theory of circuit analysis. These latter allow a possibility to estimate the rotor impedance and the phenomena generated (the influence of these pieces and the skin effect) during the frequency variation.

However, in order to well predict the transient behavior of these modified IM. A dynamic equations system, with variable parameters, has been presented which allow to take into consideration these phenomena.

2. Theoretical study

The deep bars were introduced to improve the starting characteristics of induction motors, due to their height of slots, the skin effect phenomenon manifests itself very strongly (for more than 13*mm* for copper and more than 19*mm* for aluminum conductors [1]) and significantly changes the rotor parameters. The current density flows through the bars with a non-homogeneous dissipation, when the frequency is high, the current tends to circulate on the periphery of the conductor, thus forming a skin surfaces. An increasing in resistance and a decreasing in the leakage reactance causing a low current call and a high starting torque (i.e. a reduced start-up time).

These actuators are less costly and simple to perform compared to those of double cages, however, this latter remains the configuration, which has better start-up characteristics. In order to approach its characteristics (in the case of a deep bar), this article proposes to design a deep bar that is more efficient

than a double cage without affecting its dimensions. This is achieved by means of insertion of the solid ferromagnetic pieces inside it.

To justify the approach followed, three modified IM bars [18] have been analyzed and compared to this of double cage (which presents better performances at the start-up). Figure (1) illustrates their respective dimensions.

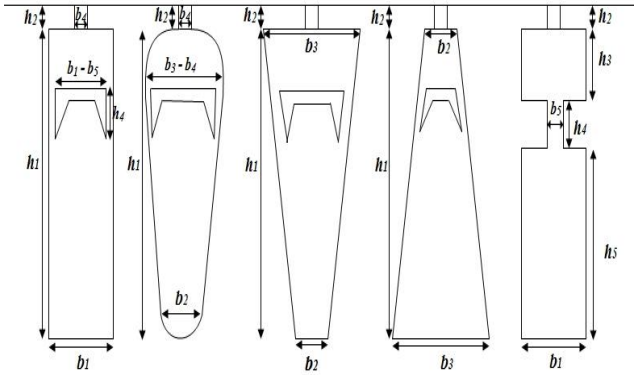

Fig. 1. Geometry dimensions of the bars forms studied

Where: h_1=29.5*mm*, h_2=0.7*mm*, h_3=9.5*mm*, h_4=4*mm*, h_5=20.5*mm*, b_1=5.7*mm*, b_2=4*mm*, b_3=7*mm*, b_4=0.5*mm* and b_5=1.5*mm*. The bars section is equal to 169 mm^2 and the conductivity of the Aluminum (conductor) is equal to 34,5.10^6 $S.m^{-1}$ (at 300*k*) and that of the piece (steel) is equal to 5,9.10^6 $S.m^{-1}$ (at 300*k*).

The main dimensions of the simulated motors are presented in the table 1 [18].

Table 1. Dimensions of the IM studied

Phase, Pole	3*Ph*, 4*Pole*
Output power	15*kW*
Primary voltage	220 *V*, 50 *Hz*
Stator diameter	272 *mm*
Rotor diameter	184 *mm*
Air gap	1 *mm*
Stator and rotor slots number	48, 38 *slots*
Core length	247 *mm*
Nominal currant	29.2 *A*
Rated speed	1455 *rpm*
X_s	1.754 Ω
R_s	0.302 Ω
$X_r^{'}$ (without skin effect)	1.443 Ω
$R_r^{'}$ (without skin effect)	0.298 Ω
X_m	39.21 Ω
R_m	3.622 Ω

These structures have been analyzed by the field calculation, using the numerical approach, which is presented below.

3. Numerical method

Finite element modelling (FEM) is the most relevant means for the study of electromagnetic phenomena and their visualization. As a result, several software packages have been designed using FE analysis, which offers the possibility of performing complex calculations and approximating physical phenomena with large precision, as in the case of processing arbitrary form systems consisting of several different material regions [25].

Furthermore, it is possible to take into account the geometrical deformation, the non-linearity of the materials and the skin effect in the rotor bars, using the FEM, as reported in the work in [12, 17, 19].

However, a complete analysis of the IM requires a considerable time computation for a simple impedance calculation. Nevertheless, it is possible to carry out a single bar analysis in the case of a resolution of magneto-harmonic hypothesis to estimate these phenomena. To do this, the boundary conditions must be well defined in such a way to reproduce the conditions that the bars are subjected in a complete analysis of the IM, for that the following assumptions are applied:

- The Neumann conditions $\left(\frac{\partial \vec{A}}{\partial \vec{n}} = 0\right)$, are applied on the left and right sides of the bar, in order to have the field lines perpendicular to the faces of the bars (to force the flux to cross the border with a 90° degree angle);
- The Dirichlet conditions $\left(\vec{A} = 0\right)$ are applied to the upper and lower sides, to force the flux to be parallel to the boundary [23].
-

3.1. Simulation results under FEMM

Encouraged by the various successes achieved so far, for the rotor impedance computation, by the finite element method [18], this latter has been applied, in the same concept, to arbitrary modified rotor bars shapes (Figure (1)), which lodged a massive ferro-magnetic part in their interiors. The obtained results are illustrated in the figures (3 to 6):

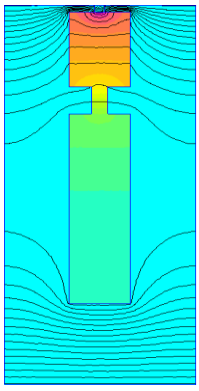

(a) 50 Hz

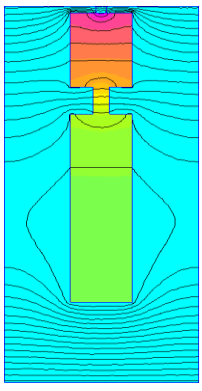

(b) 20 Hz

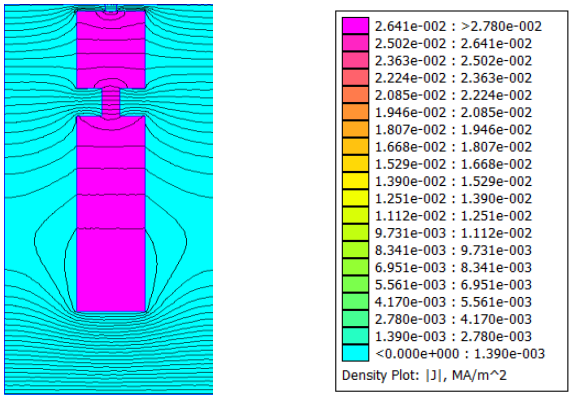

(c) 5 Hz

Fig. 2. Current densities and field lines in double cage bar at different frequencies.

Figure (2) shows the simulation results for a double cage bar at different frequency values. According to (a) and (b) (at f = 50 Hz) the upper part of the bar has a high current density compared to the lower one, which is almost zero. This induced an increasing of the bar resistance (the bar section is reduced). In the case of (c) when the frequency decreases the current density is distributed uniformly over the entire cross section of the bar, the resistance in this case is low.

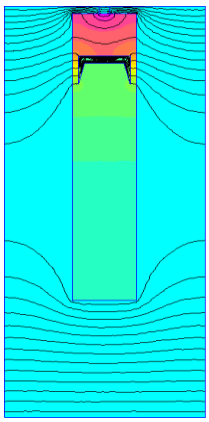

(a) 50 Hz

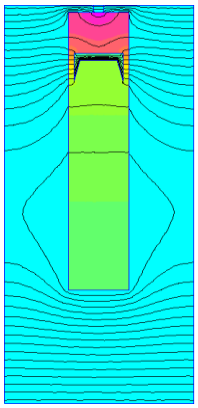

(b) 20 Hz

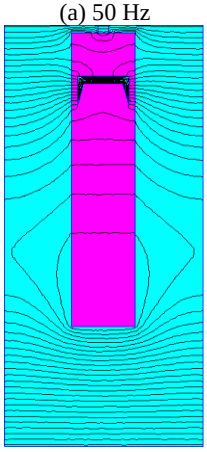

(c) 5 Hz

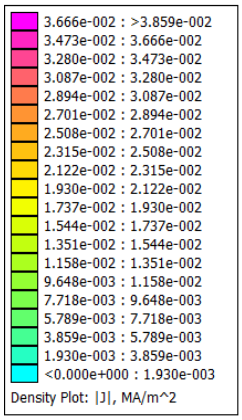

Fig. 3. Current densities and field lines in rectangular bar with piece at different frequencies

Figure (3) shows a modified deep rectangular bar (which lodged a solid ferromagnetic piece inside). In the case of the high frequency (a) and (b), the field lines are delimited by this piece, they are focused on the upper part of this latter, which causes an accentuation of a non-uniform penetration of the current density. In addition, this forces the current to circulate on the conductor periphery, because of its high electrical resistivity, inducing a large resistance value (behaving like the upper double cage slot (Fig.2)). Elsewhere, the leakage inductance of the upper part is negligible (compared to the high value of the resistance). At low frequency values. I.e. in case of (c), the piece becomes saturated and unnecessary, allowing the currents to flow through the entire section of the bar.

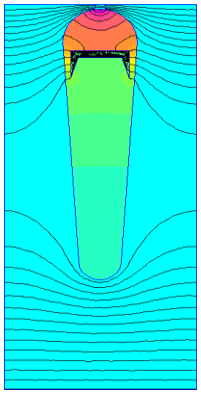

(a) 50 Hz

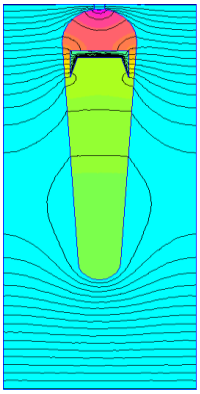

(b) 20 Hz

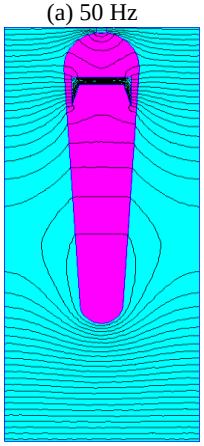

(c) 5 Hz

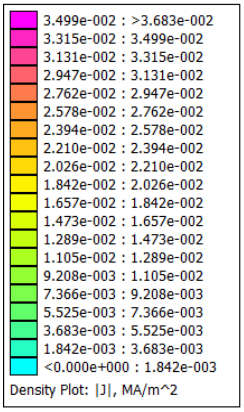

Fig. 4. Current densities and field lines in modified oval bar at different frequencies.

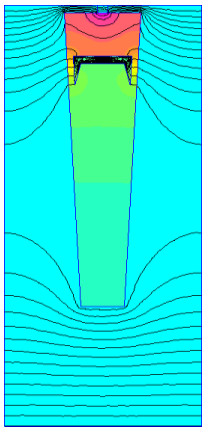

(a) 50 Hz

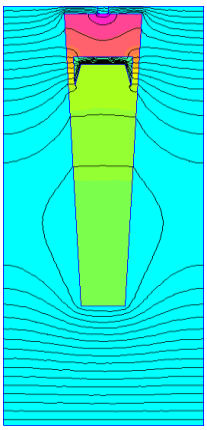

(b) 20 Hz

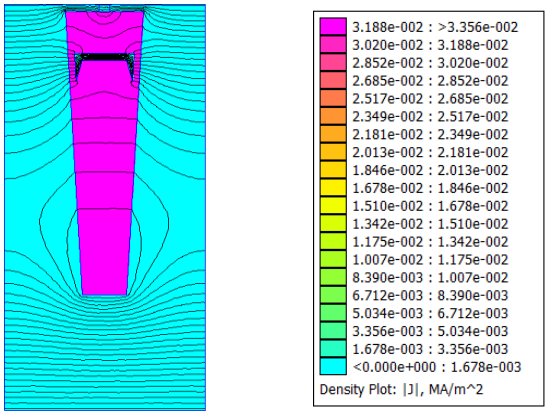

(c) 5 Hz

Fig. 5. Current densities and field lines in modified trapezoidal bar at different frequencies

Figures (4) and (5) illustrate modified oval and trapezoidal deep bars respectively. As in the previous case, this form has the same propagation shape of the field lines and the current density distribution. Despite the same piece layout as the previous bar (rectangular shape), the values obtained from the current density in this case, are less important. This is due to its geometric shape, which has a large section in the air gap direction. The bar resistance value will become less important in this case.

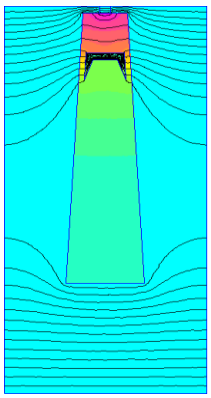

(a) 50 Hz

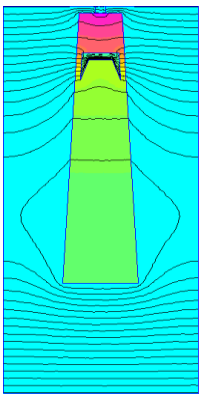

(b) 20 Hz

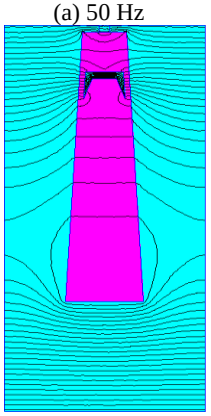

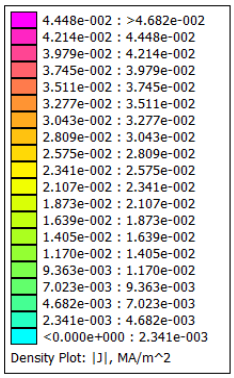

(c) 5 Hz

Fig. 6. Current densities and field lines in modified trapezoidal inverted bar at different frequencies

From figure (6), the bar present a high value of the current density at the start (a) compared to others forms, one can see that, the bar shape has strongly influenced the rotor parameters. One can find such bars in the IM external rotor with great performances.

From these results, it can be seen that the geometrical deformation of the bars is taken into account and also the massive pieces inserted, which delimit the propagation of the current density and promote the manifestation of the skin effect phenomenon. This causes a decrease in the conduction section, which increase the bar resistance. Consequently, the IM performances will improved. Moreover, these bar's forms have an advantage over that of the double cage

• From the electrical point of view; these contribute to the induction and conduction of the currents in the bars by means of its electrical conductivity;

• From the magnetic point of view; it favors the passage of the field lines, allowing an important number of them to pass, while delimiting it on the lower part of the bar, as observed in the figures (3-6). Characterized by a high electrical resistivity equal to $13.10^{-8}\Omega.m$ (approximately 5 times greater than that of Aluminum), the equivalent resistance in this case is significant, which reduces the current demand and improves the torque at startup.

• The position and shape of the piece are selected in such a way as to obtain improvements in starting performance minimizing the deterioration of its nominal operating characteristics. The choice of the frequency value (which varies from 50 Hz to 0 Hz) is set to predict the rotor impedance values in the case of IM direct coupling to the electrical network.

To argue the followed approach another method of approximation, which allows the calculation of the non-uniform displacement of the current in the rotor bars is presented below.

3.2. Semi-analytical method

The deep-bar decomposition as staircase (circuit analyses) offers the possibility to take into consideration the non-uniform current distribution (skin effect), during the frequency variation. This approach is introduced by Babb and Williams [9, 10], and Klingshirn and Jordan [11]. It is effective and can rival with FEM, in the case of bar impedance calculation [14, 15]. However, there are various configurations to interpret this bar fraction, the most used are those L, T or PI shaped. [13-16, 19]. According to [14] the last has a best configuration for a large frequency range.

A modeling with L-shaped configuration (Figure (7)), has been done for the modified bars of figure (1), following the same approach as [18].

In the steady state, referring to the figure (7) the voltage equation in the k^{th} sub-conductors is expressed as follows:

$$\dot{E}_k = -j\omega\Delta\Phi_k = R_k\dot{I}_k - R_{k+1}\dot{I}_{k+1} \qquad (1)$$

Where: $\Delta\Phi_k$ is the leakage flow circulating between the k^{th} and $(k+1)^{th}$ sub-conductors.

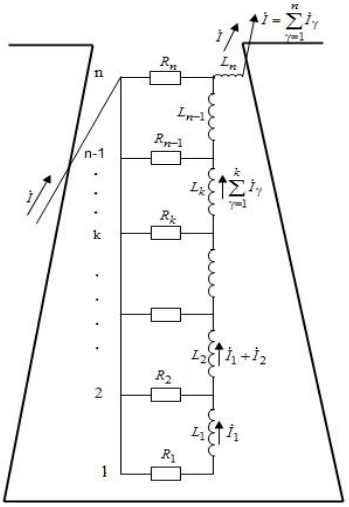

Fig.7. Trapeze bar in stair-shaped electrical circuit

The flux density B_k in the sub-conductor *k* depends on the current liaison ξ_k (F.M.M) calculated from the bottom of the slot in the sub-conductor *k*.

$$\xi_k = \int \frac{B_k}{\mu_0} dl \quad (2), \quad B_k = \mu_0 \frac{\xi_k}{b_k} = \mu_0 \frac{1}{b_k} \sum_{\gamma=1}^{k} i_\gamma \quad (3)$$

Where: b_k is the width of the slot to the position of the k^{th} sub-conductor.

$$\Delta\Phi_k = B_k l h_k = \mu_0 \frac{\xi_k}{b_k} l h_k = \mu_0 \frac{l h_k}{b_k} \sum_{\gamma=1}^{k} i_\gamma \quad (4)$$

By substituting (2) into (4), we get:

$$\dot{E}_k = -j\omega\mu_0 \frac{l h_k}{b_k} \sum_{\gamma=1}^{k} \dot{I}_k = R_k \dot{I}_k - R_{k+1} \dot{I}_{k+1} \quad (5)$$

Then, we obtain: $\dot{I}_{k+1} = \frac{R_k}{R_{k+1}} \dot{I}_k + \frac{j\omega\mu_0 l h_k}{R_{k+1} b_k} \sum_{\gamma=1}^{k} \dot{I}_\gamma$

$$= \frac{R_k}{R_{k+1}} \dot{I}_k + j \frac{\omega L_k}{R_{k+1}} \sum_{\gamma=1}^{k} \dot{I}_\gamma \quad (6)$$

The resistance and reactance of the elementary conductor *k* are:

$$\begin{cases} X_k = \omega \times L_k = \omega \times \mu_0 \dfrac{h_k l}{b_k} \\ R_k = \rho \dfrac{l}{h_k b_k} \end{cases} \quad (7)$$

If the value of the current $\dot{I}_1$ is not known, we impose an arbitrary value (for example 1A) and the rest of the currents will be resolved according to the following equations system (8) [2].

$$\begin{cases} \dot{I}_1 = 1 \\ \dot{I}_2 = \dfrac{R_1}{R_2} \dot{I}_1 + j \dfrac{\omega L_1}{R_2} \dot{I}_1 \\ \dot{I}_3 = \dfrac{R_2}{R_3} \dot{I}_2 + j \dfrac{\omega L_2}{R_3} \left(\dot{I}_1 + \dot{I}_2 \right) \\ . \\ . \\ . \\ \dot{I}_{k+1} = \dfrac{R_k}{R_{k+1}} \dot{I}_k + j \dfrac{\omega L_k}{R_{k+1}} \left(\dot{I}_1 + \dot{I}_2 + \ldots + \dot{I}_k \right) \\ . \\ . \\ . \\ \dot{I}_n = \dfrac{R_{n-1}}{R_n} \dot{I}_{n-1} + j \dfrac{\omega L_{n-1}}{R_n} \sum_{\gamma=1}^{n-1} \dot{I}_\gamma \end{cases} \quad (8)$$

To consider the massive effect of the ferromagnetic piece, equation (7) is replaced by (9) at the position where this one is placed. To do this, an algorithm under MATLAB has been developed to take into account the effect and position of the massive ferromagnetic inserted piece. In our case, the number of sub-conductors is set to n = 200.

$$\begin{cases} X_\gamma = \omega \times L_\gamma = \omega \times \mu_0 \dfrac{\Delta h_\gamma l}{b_{A_\gamma}} \\ R_\gamma = \rho_{e_\gamma} \dfrac{l}{\Delta h_\gamma \left(b_{A_\gamma} + b_{f_\gamma} \right)} \end{cases} \quad (9)$$

With: $\rho_{e\gamma} = \dfrac{\left(b_{A\gamma} + b_{f\gamma} \right) \rho_A \rho_f}{b_{A\gamma} \rho_f + b_{f\gamma} \rho_A}$

Where b_{A_γ} : aluminum conductor width; $b_{f\gamma}$: Width of the ferromagnetic massive piece; ρ_A: Resistivity of aluminum; ρ_f : Resistivity of steel.

In our case, the value of the current I_1 is equal to 1A. This way, the total current of the bar is:

$$I_b = \sum_{\gamma=1}^{n-1} \dot{I}_\gamma \quad (10)$$

The calculation of the resistance R_{be} and the leakage inductance X_{be} of the bar taking into account the skin effect, is done using expressions below [2]:

$$R_{be} = \frac{\sum_{\gamma=1}^{n}\left(I_\gamma^2 R_\gamma\right)}{I_b^2} \quad (11), \qquad X_{be} = \omega \mu_0 \lambda_{be} l \quad (12)$$

Where $\lambda_{be} = \frac{\sum_{\gamma=1}^{n}\left(\lambda_\gamma \left|\sum_{k=\gamma}^{n} \dot{I}_k\right|^2\right)}{I_b^2}$: Conductibility dispersion coefficient of the slot taking into account the skin effect [26]. The coefficients k_r and k_x which allow taking into account the variations in the resistance and the leakage inductance, respectively, are given by the equations (13 and 14):

$$k_r = \frac{R_{be}}{r_0} \quad (13), \qquad k_x = \frac{X_{be}}{X_0} \quad (14)$$

Where $r_0 = \rho \frac{l}{hb}$: The bar resistance without skin effect;

$X_0 = \omega \mu_0 l \frac{\sum_{\gamma=1}^{n}\left(\lambda_\gamma \left(\sum_{k=\gamma}^{n} q_k\right)^2\right)}{q_b^2}$: Leakage reactance without skin effect (i.e. uniform current distribution). While $\sum_{k=\gamma}^{n} q_k$ is the sum of the of the elementary conductors sections [26].

4. Interpretation results

The two approaches outlined above, effectively describe the behavior of the resistance and leakage reactance, interpreted as two coefficients k_r and k_x of each shaped bar studied. A comparative analysis has been made between the two methods, in order to estimate the relative error between them. The simulation results are illustrated below.

The evolution of k_r and k_x coefficients for a double cage bar are presented in figures (8, 9).

The figures (8, 9) show the evolution of the two coefficients k_r and k_x versus slip in the case of a double cage bar. They exhibit an exponential important value. That is means the rotor parameters are clearly infected.

The relative error is determined by equation (15):

$$Relative\_error\% = 100 \times \left|\frac{k_{nn} - k_{nc}}{k_{nn}}\right| \quad (15)$$

With k_{nn} : (k_r or k_x) coefficient for numerical solution; k_{nc} : (k_r or k_x) for circuit analysis solution.

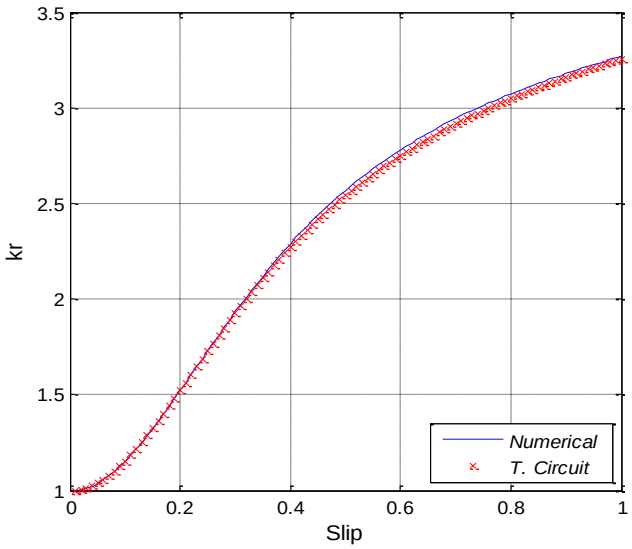

Fig. 8. k_r evolution of double cage bar versus slip

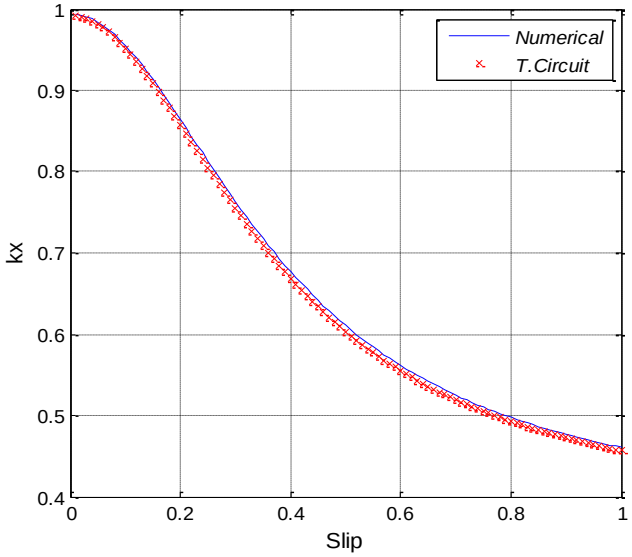

Fig. 9. k_x evolution of double cage bar versus slip

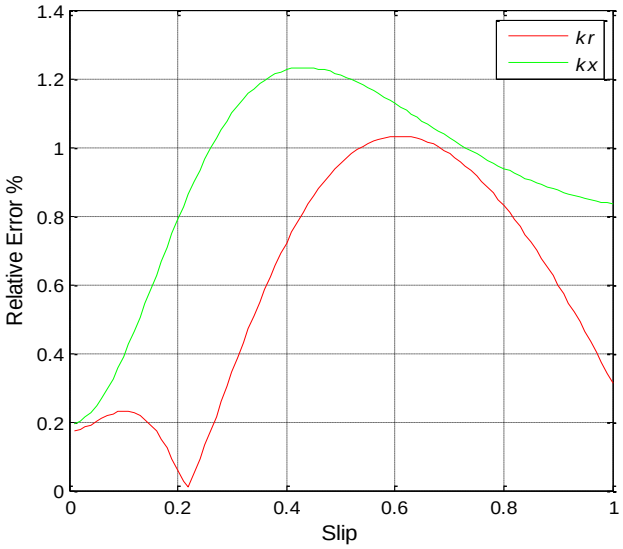

Fig. 10. Relative error in function of the slip

From figure (10), the approach followed is argued by the fact that the maximum value of the relative error of the two methods does not exceed 1.22% this is valid for the both coefficients.

The evolution of k_r and k_x for a rectangular bar with piece are presented in figures (11, 12).

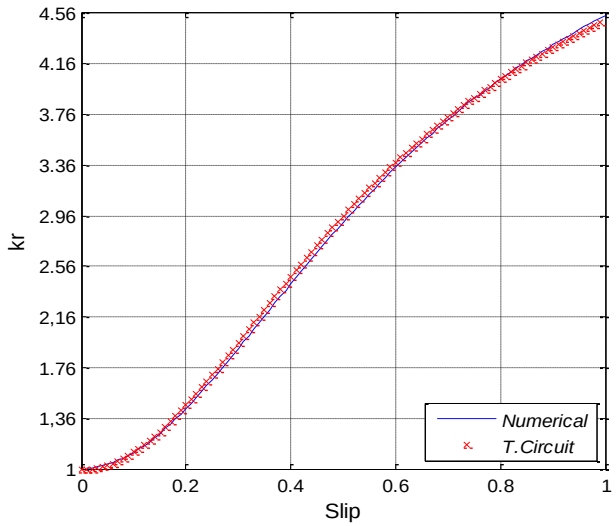

Fig. 11. k_r evolution of modified rectangular bar versus slip

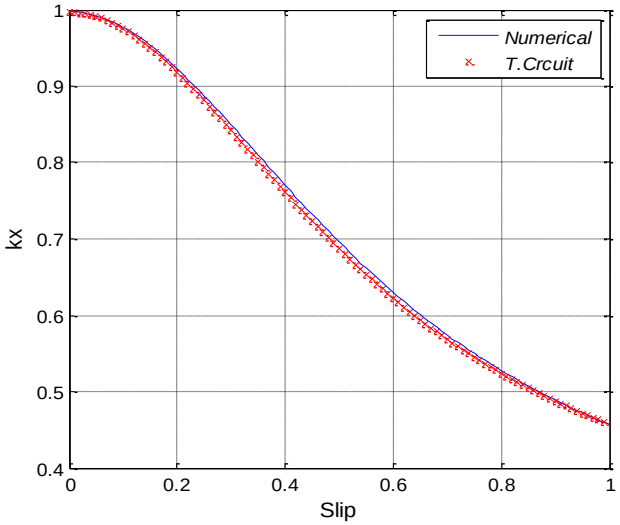

Fig. 12. k_x evolution of modified rectangular bar versus slip

According to figures (10, 11) the two coefficients k_r and k_x evolve in the same way as those previously obtained. However, a higher value of the k_r coefficient is noticed at s =1, the bar resistance is multiplied by 4. 56. For k_r coefficient this one is low in high slip value the reactance in this case is low.

From figure (13), the maximum relative error of the two methods remain at least constant about 1.25%.

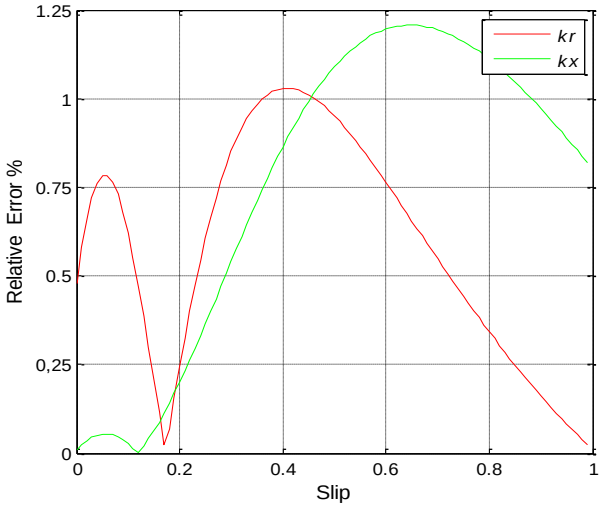

Fig. 13. Relative error in function of the slip

For the oval bar with piece, the evolution of two coefficients are presented in figures (14, 15).

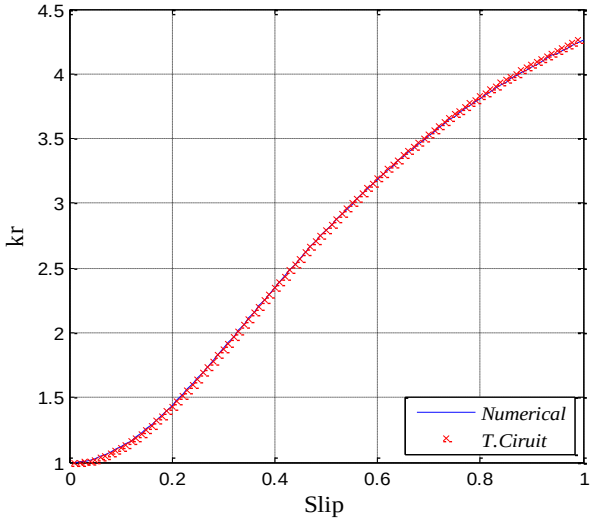

Fig. 14. k_r evolution of modified oval bar versus slip

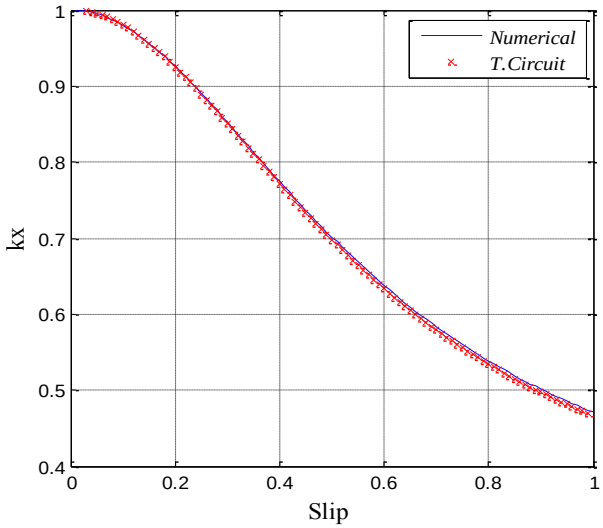

Fig. 15. k_x evolution of modified oval bar versus slip

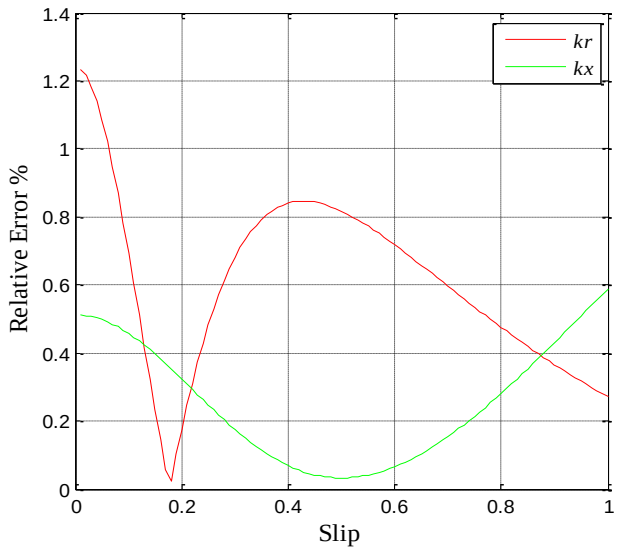

Fig. 16. Relative error in function of the slip

According to figures (14, 15), in the case of modified oval bar, the k_r coefficient has small undergone a decrease compared to the latter one, this is explained by its large cross-section in the vicinity of the air gap. However, the k_x coefficient varies insignificantly.

According to figure (16), the relative error has slightly increased its maximum value is in the neighborhood of 1.2%.

For the trapezoidal bar with piece, the evolution of two coefficients are presented in figures (17, 18).

In the case of figure (17), there was a slight decrease in the k_r value, which is almost equal to that of double cage. From the figure (18), the coefficient k_x varies in the same way as those previously seen with fixed values (at s = 1).

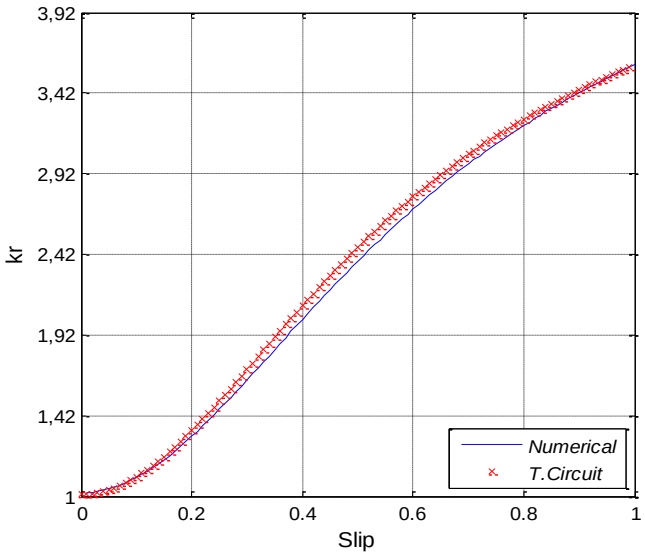

Fig. 17. k_r evolution of modified trapeze bar versus slip

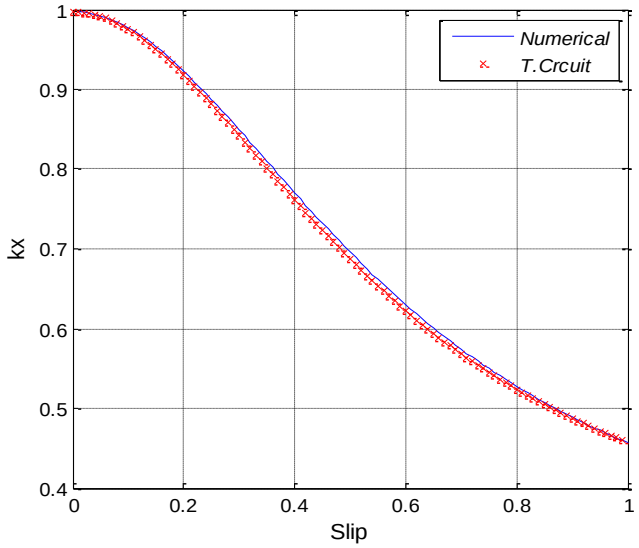

Fig. 18. k_x evolution of modified trapeze bar versus slip

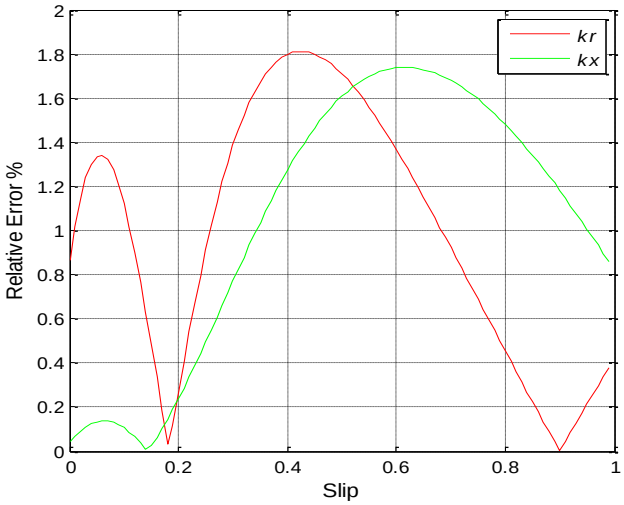

Fig. 19. Relative error in function of the slip

According to figure (19), the maximum relative error is slightly increased (1.8%). However, it is still low value.

For the trapezoidal inverted bar with piece, the two coefficients are presented in figures (20, 21).

From the figures (20, 21), it can be seen that the inverted trapezoidal bar has a larger k_r coefficient value compared with the other shapes (in the case of s = 1), this means that a large resistance value is reached, the latter has a low value at low slip (at nominal speed). In the case of k_x coefficient, this one, is at its minimum value at startup, the leakage reactance is reduced, which limits the reactive current and thus improves the power factor.

From the results it can be seen that the calculation of the skin effect can be estimated by these two presented methods, this is justified by the modest maximal value of the relative error obtained (1.8%).

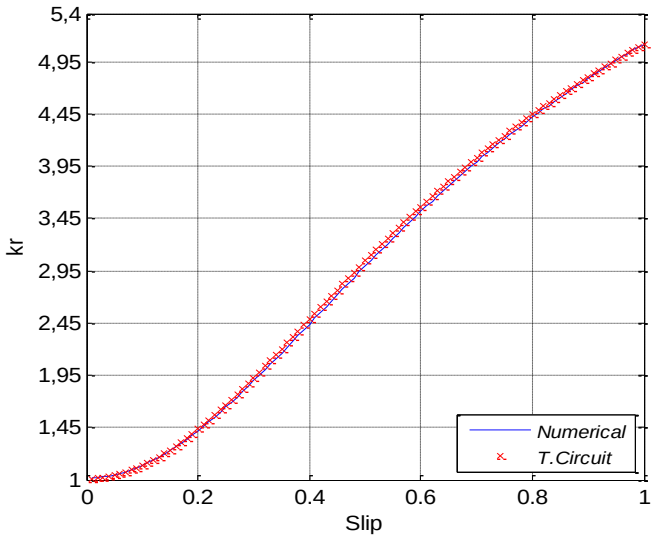

Fig. 20. k_r evolution of modified trapeze inverted bar versus slip

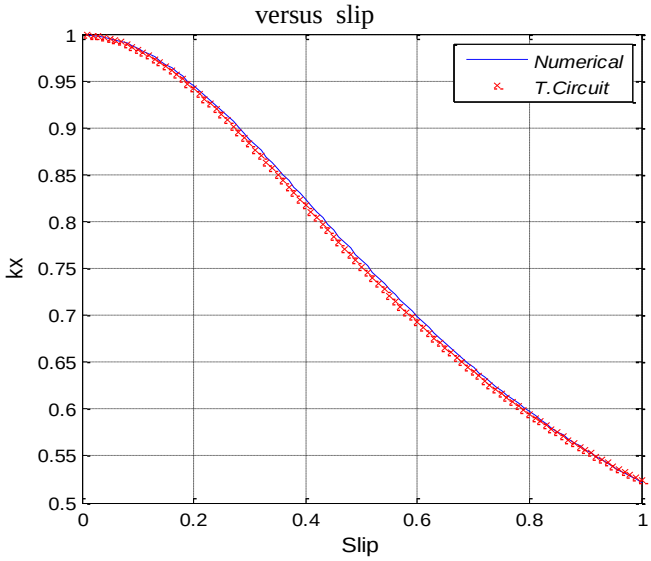

Fig. 21. k_x evolution of modified trapeze inverted bar versus slip

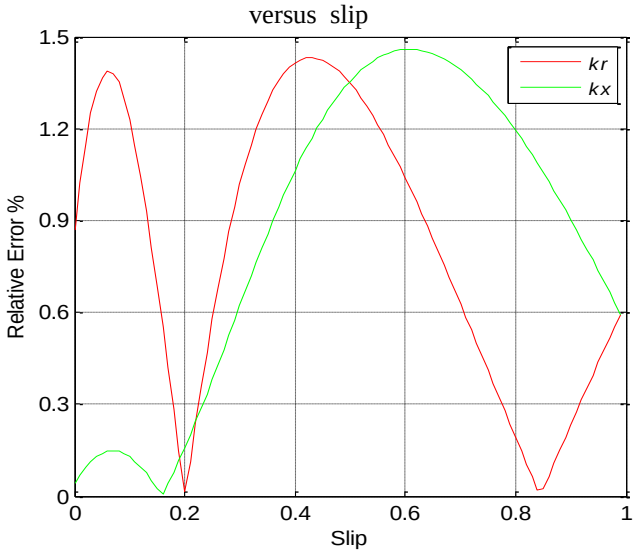

Fig. 22. Relative error in function of the slip

However, the two coefficients calculated above, which refer to the bar resistance and the leakage reactance, evolve tangibly, such a variation certainly cannot be neglected. For this purpose an approximation of these latter by the least squares method is performed, expressing a polynomial of order six, which is a function of the slip, this one was introduced in a dynamic modeling of IM in order to include their behavior during the frequency variation.

5. Dynamic modelling

In order to predict the transient behavior of the IM a corrections have been made to the dynamic modelling including the rotor variation parameters (bar resistance and leakage reactance). A dynamic model is presented in the *dq* reference frame (Park transformation) expressed by equations (16-18):

$$\begin{cases} V_{ds} = R_s i_{ds} - \omega_s \varphi_{qs} + \dfrac{d\varphi_{ds}}{dt} \\ V_{qs} = R_s i_{qs} + \omega_s \varphi_{ds} + \dfrac{d\varphi_{qs}}{dt} \\ V_{dr} = \left(k_r R_b^{'} + R_f^{'}\right) i_{dr} - \omega_r \varphi_{qr} + \dfrac{d\varphi_{dr}}{dt} \\ V_{qr} = \left(k_r R_b^{'} + R_f^{'}\right) i_{qr} + \omega_r \varphi_{dr} + \dfrac{d\varphi_{qr}}{dt} \end{cases} \quad (16)$$

The stator and rotor flux are connected to current by the following equations (17).

$$\begin{cases} \phi_{ds} = L_s i_{ds} + M i_{dr} \\ \phi_{qs} = L_s i_{qs} + M i_{qr} \\ \phi_{dr} = \left(\left(k_x l_b^{'} + l_f^{'}\right) + M\right) i_{dr} + M i_{ds} \\ \phi_{dr} = \left(\left(k_x l_b^{'} + l_f^{'}\right) + M\right) i_{qr} + M i_{qs} \end{cases} \quad (17)$$

R_s: Stator phase resistance ; L_s: stator cyclic inductance ; M : Cyclic mutual inductance between the stator and the rotor ; $R_b^{'}$ and $l_b^{'}$: Resistance and leakage inductance of the bar portion turned to stator respectively, traversed by a uniform current; $R_f^{'}$ and $l_f^{'}$: Resistance and leakage inductance of the frontal part of the bar turned to stator respectively.

The electromagnetic torque is given as a function of the stator flux and current by the following expression:

$$T_e = p\left(\phi_{ds} i_{qs} - \phi_{qs} i_{ds}\right) \quad (18)$$

5.1. Simulation results

The electromechanical characteristics of the IM studied are presented below in the case of direct coupling to the electrical network, carrying out under MATLAB/Simulink environment. The results obtained are given in figures (23-26).

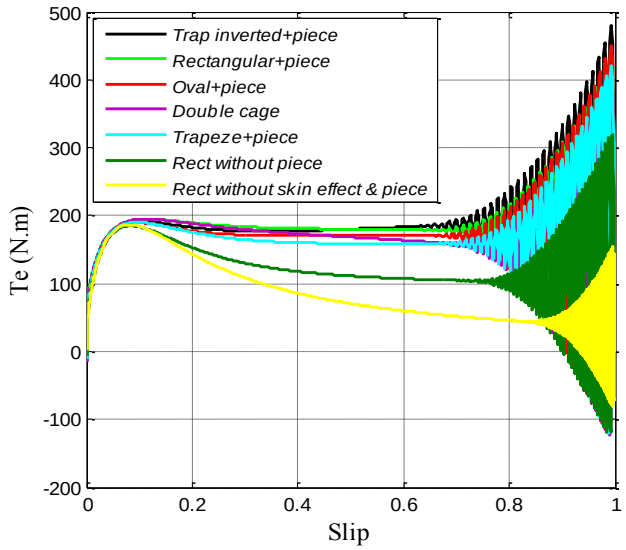

Fig. 23. Torque evolution in function of the slip

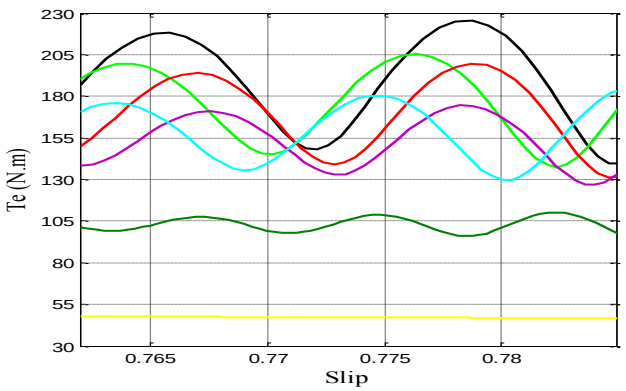

Fig. 24. Torque's curve zoom versus slip

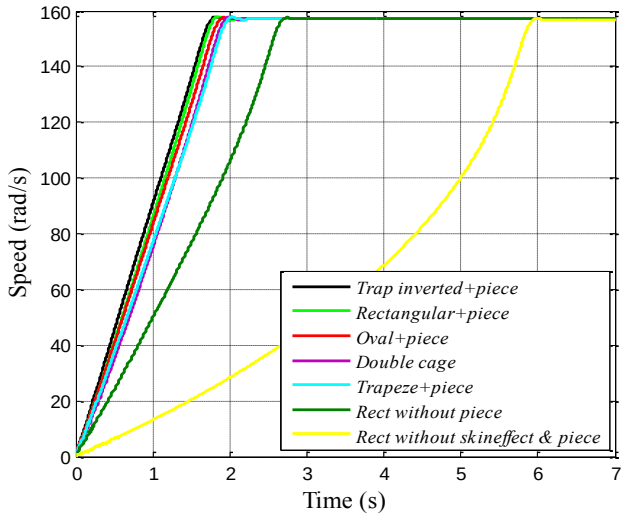

Fig. 25. Evolution of torque in function of the slip

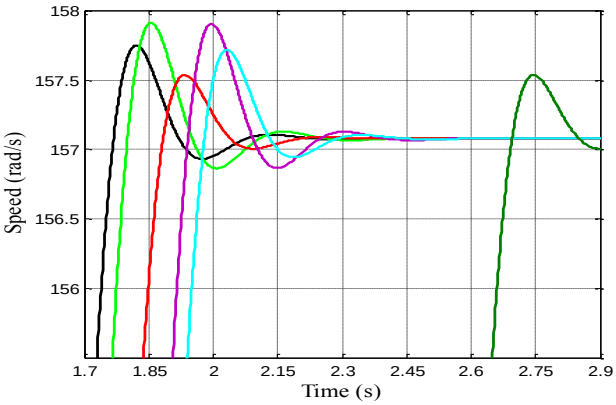

Fig. 26. Speed's curve zoom versus time

5.2. Interpretation results

Figures (23, 26) illustrate the electromechanical characteristics of motors with the different rotor bars previously seen. Referring to the curves without skin effect, we can note that the IM develops a low starting torque and takes a long time to start. However, in the case where the skin effect is taken into account, the characteristics of IM are significantly improved, the developed starting torque is almost multiplied by *2* and the startup time is reduced by 3.5 seconds. It means that the classical modelling of the IM does not give precise results.

In the case of the various motors with presence of these ferromagnetic pieces, a powerful improvement in the starting performance and the IM dynamics is obtained. In the case of the rectangular bar with piece, the starting torque is improved by 100 *N.m* compared with that without the piece (with the green color). This one even exceeding the double cage IM performances.

In addition, for motors with trapezoidal bar, which generally found in the case of small/medium power (does not require a high starting torque) can now compete with those of double cage motors, according to the results obtained the performances of the two motors are the same. They even can replace them because their dimensions are lower than those of double cage.

Note: In our case the inertia is equal to $J = 2\ kg.m^2$ in order to have better visualization for the speed evolution.

6. Conclusion

A series of deep bars motor, with the same power, have been modified in order to improve their performances. This is done by placing massive ferromagnetic pieces inside the rotor bars, to increase their resistances. Moreover, the role of those pieces is

to delimit the induced currents displacement above them. Consequently, the bar section is reduced and its resistance increased. Those latter also contribute to inducing currents because of their electrical conductivity.

However, its dimensions and shape are chosen such as to find compromises between IM startup and nominal operation.

However, the two used approaches, which take into account the influence of these ferromagnetic pieces and the skin effect, offer a good accuracy, this is justified by the maximum value of the relative error, which does not exceeds 1.8% for all bar forms analyzed.

Moreover, the transient performances of the motors studied (with pieces) exceed widely (in the case of the same power) those of the double cage motors (at starting). In addition, a reduction in the dimensions of these actuators is achieved compared to the latters, thus offering a reduction in the cost and the possibility of increasing their applications.

References

1 Kostenko M., & Piotrovski, L.: (*Machines électriques Tome II)* éditions mir, Moscou, Russia, 1979.

2 Pyrhönen, J., Jokinen, T., & Hrabovcovà, V.: (*Design of rotating electrical Machines)*, Wiley, 2008.

3 Levi, E.: *Impact of cross-saturation on accuracy of saturated induction machine models*. In: IEEE Transactions on Energy Conversion (1997), vol. 12, No 3, p. 211-216.

4 Akbaba, M., and S. Q. Fakhro.: *Saturation Effects in Three-phase Induction Motors*. In: Electric machines and electro-mechanics (1987), vol. 12, no 3, p. 179-193.

5 Mademlis, Christos, & Vassilios G. Agelidis.: *On considering magnetic saturation with maximum torque to current control in interior permanent magnet synchronous motor drives*. In: IEEE transactions on energy conversion (2001), vol. 16, no 3, p. 246-252.

6 Costin, M., Dobrota, I., & Voncilă, I.: *Thermal approach of aspect ratio on design of electrical machines.* In: Scientific Bulletin of the Electrical Engineering Faculty; 2013, No.2 vol.22.

7 Xyptras, J., and V. Hatziathanassiou.: *Thermal analysis of an electrical machine taking into account the iron losses and the deep-bar effect*. In: IEEE Transactions on Energy Conversion (1999), vol. 14, no 4, p. 996-1003.11.

8 Mezani, Smail, N. Takorabet, and B. Laporte.: *A combined electromagnetic and thermal analysis of induction motors*. In: IEEE Transactions on Magnetics (2005), vol. 41, no 5, p. 1572-1575.

9 Babb, D. S., and J. E. Williams.: *Circuit analysis method for determination of AC impedances of machine conductors*. In: Transactions of the American Institute of Electrical Engineers (1951), vol. 70, no 1, p. 661-666.

10 Williamson, S., and M. J. Robinson.: *Calculation of cage induction motor equivalent circuit parameters using finite elements*. In: IEE Proceedings B (Electric Power Applications). 276IET Digital Library, 1991, vol. 138, no. 5, p. 264-276.

11 Klingshirn, Eugene A., and Howard E. Jordan.: *Simulation of polyphase induction machines with deep rotor bars*. In: IEEE Transactions on Power Apparatus and Systems 6 (1970), no. 6, p. 1038-1043.

12 Khang, H. V., and A. Arkkio.: *Parameter estimation for a deep-bar induction motor*. In: IET electric power applications (2012), vol. 6, no. 2, p. 133-142.

13 Wu, X., & Wang, X.: *Parameter calculation for induction machine rotor bar with non-sinusoidal current*. In: Electrical Machines and Systems, 2005. ICEMS 2005. Proceedings of the Eighth International Conference IEEE, 2005, Vol. 1, pp. 60-63.

14 Levy, W and Landy, C. F and McCulloch, M.: *Improved models for the simulation of deep bar induction motors*. In: IEEE Transactions on Energy conversion. (1990), vol. 05, no. 02, pp 393–400.

15 Benecke, Marcel, & al. *Skin effect in squirrel cage rotor bars and its consideration in simulation of non-steady-state operation of induction machines*. In: PIERS online (2011), vol. 7, p. 5.

16 Boglietti, A., Andrea C., and M. Lazzari. : *Algorithms for the computation of the induction motor equivalent circuit parameters-Part II*. In: Industrial Electronics. 34th Annual Conference of IEEE, (2008). p. 2028-2034.

17 Gheorghe, Cristina Mihaela.: *Numerical modeling approaches for the analysis of squirrel-cage induction motor*. In: Rev. Roum. Sci. Techn.–Électrotechn. et Energ (2016), vol. 61, no 1, p. 18-21.

18 Z. Maddi and D. Aouzellag. : *Dynamic Modelling of Induction Motor Squirrel Cage for Different Shapes of Rotor Deep Bars with Estimation of the Skin Effect*. In: Progress In Electromagnetics Research M, (2017), vol. 59, , p.147-160.

19 Rahimpour, E., Vahid, R., and Mahmood P.: *Parameter identification of deep-bar induction motors using genetic algorithm*. In: Electrical Engineering (Archiv fur Elektrotechnik) (2007), vol. 89, no 7, p. 547-552.

20 Kim, Young Sun.: *Analysis of Starting Torque and Speed Characteristics for Squirrel Cage Induction Motor According to Material Properties of Rotor Slot*. In: Transactions on Electrical and Electronic Materials (2015), vol. 16, no 6, p. 328-333.

21 Yetgin, Asim Gokhan, and Mustafa Turan.: *Effects of Rotor Slot Area on Squirrel Cage Induction Motor Performance*." In: International Journal of Innovative Science, Engineering & Technology, November 2016, Vol. 3 Issue 11.

22 Zhang, Dianhai, Chang Soon P., and Chang S., K.: *A new optimal design method of rotor slot of three-phase squirrel cage induction motor for NEMA class D speed-torque characteristic using multi-objective optimization algorithm*. In: IEEE transactions on magnetics (2012), vol. 48, no 2, p. 879-882.

23 Z. Maddi, D. Aouzellag and T. Laddi.: *Influence of the skin effect and the form of slot on the starting characteristics of induction motor squirrel cage*. In: Recent Advances in Mechanics, Mechatronics and Civil, Chemical and Industrial Engineering.2015, pp. 125-129.

24 Lee, G., Min, S., & Hong, J. P.: *Optimal shape design of rotor slot in squirrel-cage induction motor considering torque characteristics*. In: IEEE Transactions on Magnetics (2013), vol. 49, no 5, p. 2197-2200.

25 Zienkiewicz, O. C., Taylor, R. L., Zienkiewicz, O. C., & Taylor, R. L.: *(The finite element method)*, McGraw-hill London, 1977.

26 Kopilov. I. P.: *(Calculation of the electric machines)*, Moscou, Russia, 2002.